


 CrossMark
click for updates

 Cite this: *CrystEngComm*, 2014, 16, 8064

Synthesis of In_2S_3 microspheres using a template-free and surfactant-less hydrothermal process and their visible light photocatalysis†

 Arpan Kumar Nayak,^a Seungwon Lee,^b Youngku Sohn^b and Debabrata Pradhan^{*a}

Indium sulfide (In_2S_3) microspheres of (β -) tetragonal phase were synthesized by varying the indium precursors using a template-free and surfactant-less hydrothermal process at 150 °C. The as-synthesized samples were found to be crystalline and phase pure as confirmed by X-ray diffraction and X-ray photoelectron spectroscopy studies, respectively. Indium precursors play an important role in controlling the shape of the building blocks, *i.e.* nanoflakes or nanobricks, of In_2S_3 microspheres. The photocatalytic activity of as-synthesized In_2S_3 microspheres was tested for the degradation of methylene blue and crystal violet in the presence of visible light produced by an incandescent lamp. The terephthalic acid test using photoluminescence spectroscopy shows hydroxyl radicals as active species for the degradation of organic contaminants. Repeat photocatalysis measurements suggest the high stability of In_2S_3 microspheres without a change in their morphology and phase.

 Received 21st April 2014,
Accepted 8th July 2014

DOI: 10.1039/c4ce00836g

www.rsc.org/crystengcomm

1. Introduction

Metal oxide semiconductors are extensively used in photocatalysis. However, the wide band gaps of most oxide semiconductors limit their photocatalytic and photovoltaic applications. This is due to a small percentage (~5%) of ultraviolet (UV) radiation in the solar spectrum. Therefore, it is indispensable to explore semiconductor photocatalysts with narrower band gaps to be used under visible light of solar spectrum.^{1–3} Chalcogenides such as CdS, CdSe, ZnSe, ZnTe, InS, In_2S_3 , *etc.* have band gaps in the visible range solar spectrum and therefore can be a potential alternative to oxides as visible light photocatalysts. Among the chalcogenides, In_2S_3 is an important group III–VI semiconductor that has been found promising for photovoltaic applications due to its stability, desired band gap energy (2.0–2.4 eV),⁴ good transparency,⁵ and photoconducting behavior.⁶ In_2S_3 exists in three different phases at atmospheric pressure, *i.e.* the defective cubic structure α - In_2S_3 (stable up to 693 K), a defect spinel structure called β - In_2S_3 (stable up to 1027 K), and the higher temperature layered structure γ - In_2S_3 (above 1027 K).⁷ Among these, β - In_2S_3 is the most stable at room temperature. Therefore

previous reports are mostly on β - In_2S_3 , which is an n-type semiconductor and is used as a promising photoconducting material for photovoltaic cell design, in thin film solar cells as an alternative to toxic CdS,⁸ and as a photocatalytic material for the degradation of dyes.^{9–11} Phase-controlled synthesis and stabilization of a particular In_2S_3 phase at room temperature depend on the growth process (by impurity incorporation).⁷

Various architectures of In_2S_3 such as 3D flower-like structures,¹² hollow nanospheres,¹³ nanosheets,¹⁴ urchin-like nanostructures,¹⁵ and nanoflake structures¹⁶ have been prepared using microwave,¹⁷ sonochemical,¹⁸ hydrothermal and solvothermal methods.¹⁴ These solution-based techniques are particularly attractive because of their low-temperature synthesis and potential for large-scale production. In the above solution-based processes, toxic chemicals including HCl, organic solvents, reducing agents, surfactants and templates are used to a greater extent.^{9,10,16,19} The most commonly used sulfur sources in the synthesis of In_2S_3 are sulfides,²⁰ sulfur powder,²¹ sodium thiosulfate,²² dimethyl sulfoxide,¹⁹ thioglycolic acid,²³ thiourea,²⁴ and thiols.²⁵ Here, we have employed a biomolecule, L-cystine, to synthesize In_2S_3 in aqueous solution, thereby making the process greener.^{12,26} The present low-temperature hydrothermal technique employed for the synthesis of In_2S_3 microspheres is facile, cost-effective and reproducible. The photocatalytic properties of as-synthesized In_2S_3 microspheres are studied by the degradation of methylene blue (MB) and crystal violet (CV). In addition, the high stability of In_2S_3 microspheres as a photocatalyst is demonstrated.

^a Materials Science Centre, Indian Institute of Technology, Kharagpur 721 302, W. B., India. E-mail: deb@matsc.iitkgp.ernet.in

^b Department of Chemistry, Yeungnam University, Gyeongsan 712-749, Republic of Korea

† Electronic supplementary information (ESI) available. See DOI: 10.1039/c4ce00836g

2. Experimental

2.1 Chemicals

Indium(III) chloride [InCl_3], indium sulfate [$\text{In}_2(\text{SO}_4)_3$], and indium nitrate [$\text{In}(\text{NO}_3)_3$] from Spectrochem, India, oxalic acid [$\text{C}_2\text{H}_2\text{O}_4 \cdot 2\text{H}_2\text{O}$] and L-cystine [$\text{C}_6\text{H}_{12}\text{N}_2\text{O}_4\text{S}_2$] from Merck, India, and ethanol [$\text{C}_2\text{H}_5\text{OH}$] from Changshu Yangyuan Chemical, China were of analytical grade and used without further purification.

2.2 Synthesis

In_2S_3 microspheres were synthesized using a simple hydrothermal method by varying the indium precursor. In a typical synthesis process, 0.11 g of indium chloride (0.01 M) and 0.48 g of L-cystine powder were dissolved in 40 mL of distilled water and stirred for 10 min. Then 0.126 g of oxalic acid was added to the solution and stirred vigorously for 30 min at room temperature. The resultant milky white solution was then transferred to a 50 mL Teflon-lined stainless steel autoclave and was heated at 150 °C for 30 h and cooled naturally to room temperature. The precipitated black-colored product was collected by centrifugation and washed with ethanol and distilled water at least three times. The same procedure was followed to synthesize In_2S_3 microspheres with two other indium precursors (at the same molar concentration), *i.e.* indium sulfate and indium nitrate, keeping other synthesis parameters fixed. Furthermore, different indium precursors of the same concentrations (0.01 M) and L-cystine were simply stirred with and without oxalic acid at room temperature. The resultant precipitates were collected in order to compare the results with the products obtained in the hydrothermal process.

2.3 Characterization

The surface morphology of as-prepared In_2S_3 microspheres was examined using a Carl Zeiss SUPRA 40 field-emission scanning electron microscope (FESEM). Energy dispersive X-ray (EDX) measurements were carried out using a Carl Zeiss EVO 60 SEM attached to an Oxford EDS detector. The effective Brunauer–Emmett–Teller (BET) surface area of the as-synthesized samples was measured using a Quantachrome ChemBET TPR/TPD analyzer. The structural properties of the as-synthesized samples were studied with a PANalytical High Resolution X-ray diffractometer (XRD) (PW 3040/60) operated at 40 kV and 30 mA using $\text{Co K}\alpha$ X-ray (1.79 Å). The detailed microstructure of the In_2S_3 product was studied with a FEI TECNAI G2 transmission electron microscope (TEM). For X-ray photoelectron spectroscopy (XPS) measurements, we used a Thermo-VG Scientific ESCALab 250 microprobe with a monochromatic Al $\text{K}\alpha$ source (1486.6 eV) with a typical energy resolution of 0.4–0.5 eV full-width at half-maximum. Fluorescence measurements were carried out with a PerkinElmer LS 55 spectrophotometer at an excitation wavelength of 250 nm generated by a xenon lamp.

2.4. Photocatalytic study

The photocatalytic activity of the as-prepared In_2S_3 microspheres was studied by the degradation of methylene blue (MB) and crystal violet (CV) in the presence of an incandescent light bulb. 10 mg of In_2S_3 powder was suspended in a 100 mL aqueous solution of MB or CV (5×10^{-5} mol L^{-1}) and sonicated for 30 min in the dark at room temperature to obtain a complete adsorption–desorption equilibrium among water, MB/CV, and In_2S_3 photocatalyst prior to the light irradiation. The dye solution was then irradiated by a 200 W incandescent lamp (Philips) at a working distance of 100 cm. The light intensity was measured to be 500 lux in a beaker containing dye solution. The degradation of dyes as a function of irradiation time was measured using UV-vis absorption spectroscopy (PerkinElmer, Lambda 750).

3. Results and discussion

3.1. Morphology

The morphology of the as-synthesized samples was examined by FESEM. Fig. 1 shows the FESEM images of In_2S_3 microspheres prepared by varying the indium precursors. Fig. 1(a) and (b) show the FESEM images of In_2S_3 microspheres of 4–8 μm diameter synthesized using indium chloride as an indium source, L-cystine as a sulfur source and oxalic acid as a shape controlling agent. These microspheres were found to be composed of flakes with a thickness of <15 nm. This supports the results reported by Yu *et al.* recently on similar spherical-like In_2S_3 microspheres using indium chloride as an indium precursor.²⁷ Upon changing the precursor to indium sulfate with other parameters fixed, microspheres of 3–8 μm diameter were obtained as shown in Fig. 1(c, d). Moreover, several of these microspheres were found to be either with a hollow [Fig. 1(c)] or with a half-sphere concave sink [Fig. 1(d)] and most of the hollow spheres had multiple pores on their surface. Similar hollow spheres with multiple pores were reported by Zhao *et al.* using indium chloride as an indium source, cysteine as a sulphur source and dodecanethiol.²⁶ Their result indicates that dodecanethiol plays a key role in the formation of hollow spheres and reducing the length, width and thickness of nanoflakes.²⁶ Upon changing the precursor to indium nitrate, In_2S_3 microspheres [Fig. 1(e, f)] of 4–5 μm diameter were obtained. Interestingly, these microspheres were not composed of nanoflakes as in the previous cases. The magnified FESEM image [Fig. 1(f)] clearly shows the brick-shaped building blocks of these microspheres. The length and width of these bricks are measured to be in the range of 300–600 nm and 100–150 nm, respectively. This suggests that the indium precursor plays an important role in forming the shape of initial building blocks of the microspheres. The effective BET surface area of In_2S_3 microspheres was measured and found to be in the order of 167.84 $\text{m}^2 \text{g}^{-1}$ (for hollow microspheres with pores on their surface obtained using indium sulfate), >69.79 $\text{m}^2 \text{g}^{-1}$ (solid microspheres obtained using indium

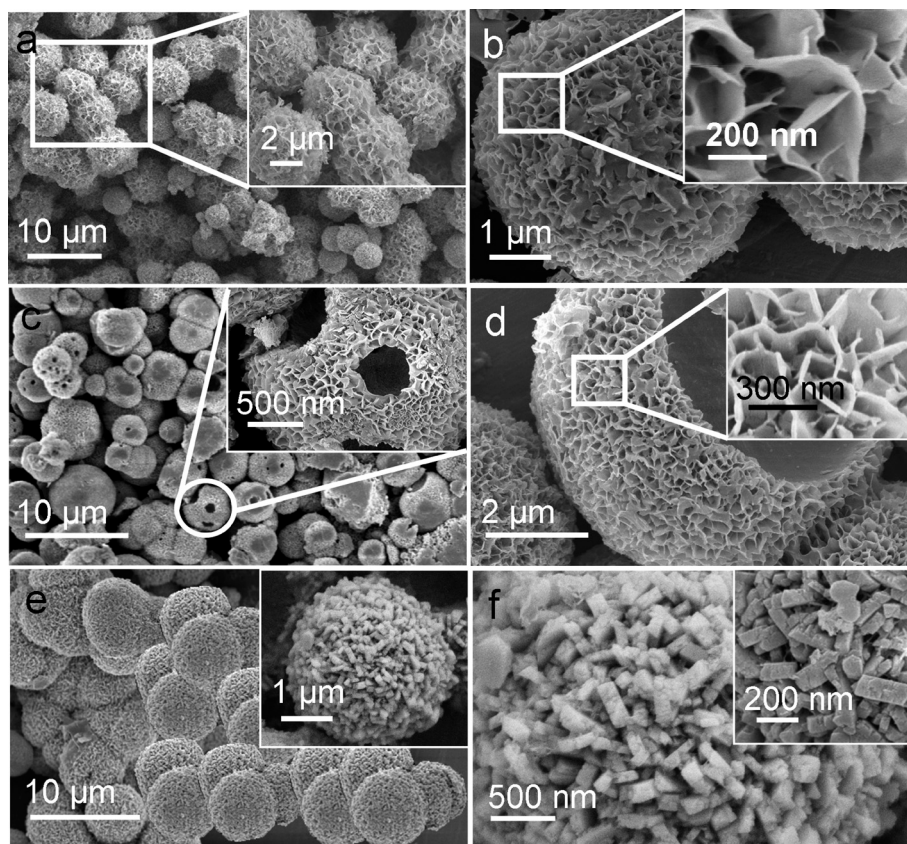


Fig. 1 FESEM images of In_2S_3 microspheres obtained at 150°C for 30 h by the hydrothermal method using (a, b) indium chloride, (c, d) indium sulfate, and (e, f) indium nitrate as precursors for indium, L-cystine for sulfur and oxalic acid as a shape-controlling agent. The inset shows the respective magnified FESEM image.

chloride) and $\gg 15.18\text{ m}^2\text{ g}^{-1}$ (solid microspheres obtained using indium nitrate). These results are well correlated to their morphology. A representative adsorption–desorption isotherm and a BJH pore size distribution plot of hollow In_2S_3 microspheres obtained with indium sulfate are shown in Fig. S1 (ESI†). The pore volume and the pore diameter were measured to be $0.813\text{ cm}^3\text{ g}^{-1}$ and 8.6 \AA , respectively, for hollow In_2S_3 microspheres.

3.2. Structural and microstructural properties

The structural properties of the as-synthesized In_2S_3 product were analyzed by powder XRD. Fig. 2 shows the XRD patterns of In_2S_3 microspheres synthesized using different indium precursors, keeping other synthesis parameters fixed. The XRD patterns match those of tetragonal $\beta\text{-In}_2\text{S}_3$ (JCPDS: 00-025-0390, upon converting to a $\text{Co K}\alpha$ source) with intense diffraction intensities from (2212), (0012) and (109) planes.¹⁶ No characteristic diffraction peaks from possible impurities such as InS , In_2O_3 , S, sulfate, and nitrate are detected, indicating phase-pure In_2S_3 product. The diffraction features are found to be slightly broad for the In_2S_3 microspheres composed of nanoflakes, which is ascribed to smaller crystallites.

The microstructure of the as-synthesized In_2S_3 microspheres was studied by TEM. Fig. 3(a) shows a TEM image of

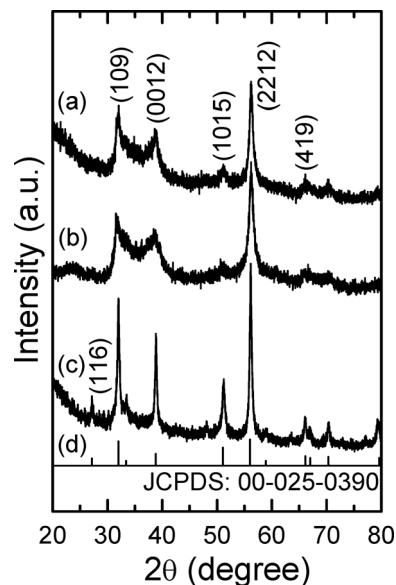


Fig. 2 Powder XRD patterns of In_2S_3 microspheres synthesized hydrothermally at 150°C for 30 h using (a) indium chloride, (b) indium sulfate, and (c) indium nitrate as indium precursors with other synthesis parameters fixed. XRD patterns were collected with a $\text{Co K}\alpha$ X-ray source. (d) A standard JCPDS file with a $\text{Co K}\alpha$ X-ray source for comparison.

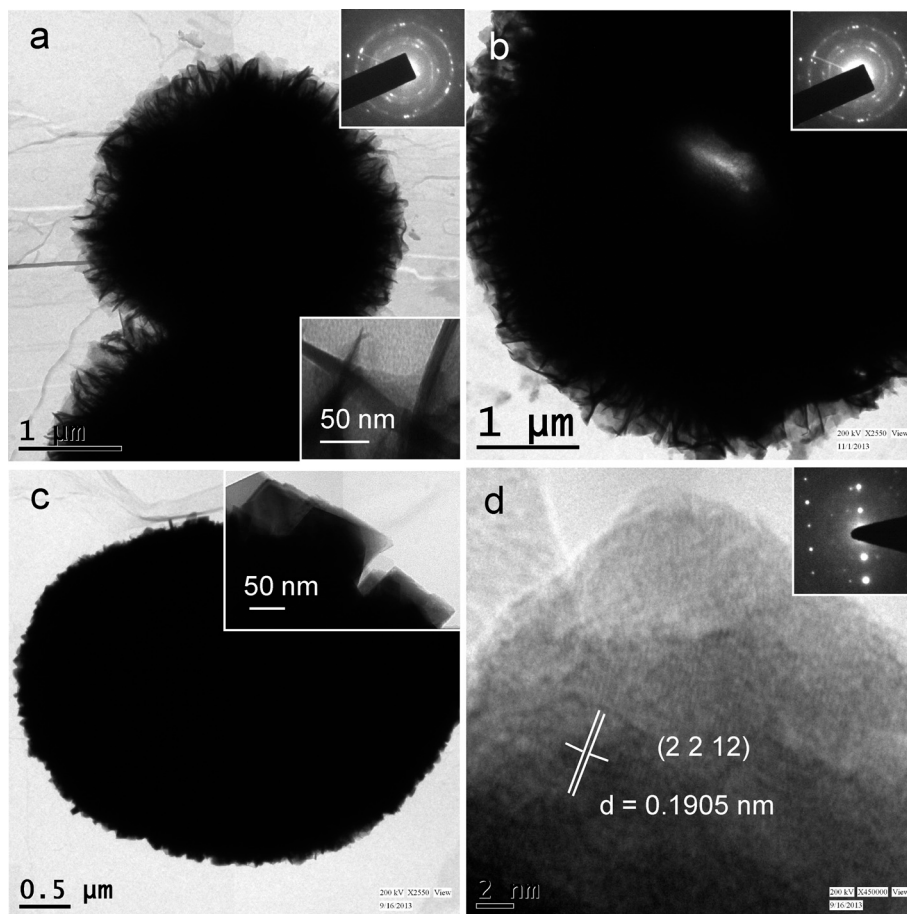


Fig. 3 TEM images of In_2S_3 microspheres obtained at 150 °C for 30 h by the hydrothermal method using (a) indium chloride, (b) indium sulfate, and (c) indium nitrate as indium precursors. (d) An HRTEM image showing the lattice fringe of the brick-shape building block of In_2S_3 microspheres shown as the inset of (c). The inset of (d) shows the corresponding SAED pattern.

In_2S_3 microspheres with a dark central part, indicating the solid nature of these microspheres. The magnified TEM image at the outer edge shown as an inset (bottom right) confirmed that these microspheres were composed of thin flake-like structures. The ring selected area electron diffraction (SAED) (top right inset) indicates polycrystalline nature of these microspheres. Fig. 3(b) represents the TEM image of In_2S_3 microspheres obtained with indium sulfate. The brighter contrast at the center of the microsphere suggests hollowness in accordance with the FESEM images [Fig. 1(c, d)]. The SAED pattern indicates polycrystalline behavior similar to that of the previous sample. Fig. 3(c) shows a TEM image of In_2S_3 microspheres obtained using indium nitrate. The TEM image clearly suggests the compact nature of these microspheres composed of nanobricks. The inset of Fig. 3(c) shows the brick-shaped building blocks of the microspheres. Fig. 3(d) shows a high-resolution TEM (HRTEM) image of a part of a nanobrick with a lattice spacing of 1.9 Å corresponding to the (2212) plane of tetragonal In_2S_3 , which has maximum XRD intensity [Fig. 2(c)]. The spot SAED pattern [inset Fig. 3(d)] further confirms the single crystalline nature of In_2S_3 nanobricks with a tetragonal crystal structure.

3.3. Composition and chemical states

EDX analysis was performed on as-prepared In_2S_3 microspheres to identify the elements present and measure their composition. Fig. 4 shows the EDX spectra of In_2S_3 microspheres synthesized with different indium precursors. The stoichiometric ratios (S:In) were measured to be 1.57, 1.54, and 1.42 for the In_2S_3 microspheres obtained with indium chloride, indium sulfate and indium nitrate, respectively. The stoichiometric ratios (S:In) are close to 1.5, suggesting the formation of In_2S_3 .

The chemical state of the as-synthesized samples was further characterized by XPS analysis. Fig. 5 shows the XPS survey spectra of In_2S_3 microspheres [Fig. 1(c, d)] obtained with indium sulfate precursor. The XPS survey spectrum shows the presence of In, S, O, and C elements, matching the literature results.²⁸ The C 1s and O 1s peaks were assigned to surface impurity carbon and adsorbed oxygen, respectively. The atomic ratio of [S]:[In] was estimated to be 1.58 from the survey spectrum confirming In_2S_3 . The left and right insets of Fig. 5 show In 3d and S 2p high-resolution region spectra, respectively. Two strong photoelectron peaks at binding energies of 444.4 and 451.9 eV are assigned to In 3d_{5/2}

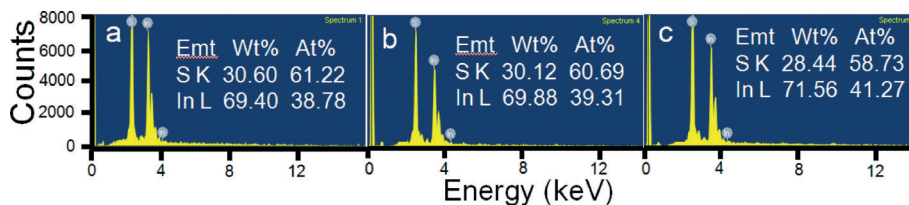


Fig. 4 EDX spectra of In_2S_3 microspheres obtained hydrothermally using (a) indium chloride, (b) indium sulfate, and (c) indium nitrate at 150 °C with other synthesis parameters constant.

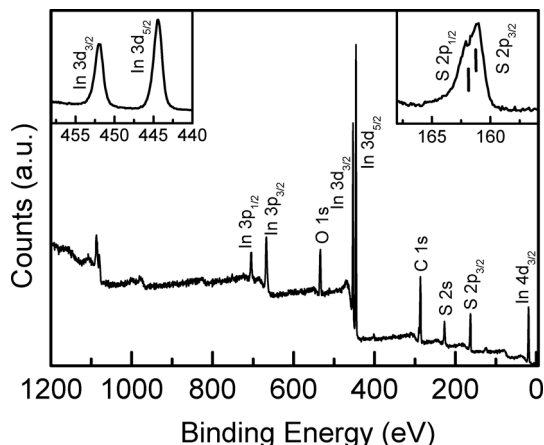


Fig. 5 XPS survey spectrum of hollow In_2S_3 microspheres hydrothermally synthesized using indium sulfate precursor at 150 °C. Left and right insets show In 3d and S 2p XPS region spectra, respectively.

and In $3d_{3/2}$ transitions, respectively, with a spin–orbit splitting of 7.5 eV. The XPS binding energy feature at 161.0 and 162.1 eV is assigned to the S $2p_{3/2}$ and S $2p_{1/2}$ transitions, respectively. These values are in good agreement with the reported data for In_2S_3 .^{29,30}

3.4. Optical properties

The optical properties of the black In_2S_3 product obtained using different indium precursors were measured by UV-vis absorption spectroscopy. The Kubelka–Munk reflectance spectra (Fig. S2, ESI[†]) of In_2S_3 microspheres synthesized using different indium precursors show strong absorption in the UV-vis region without any clear band edge. The strong absorption in the visible region of electromagnetic radiation suggests the potential use of In_2S_3 as a visible light photocatalyst.

3.5. Growth mechanism

In order to understand the growth mechanism of In_2S_3 microspheres, we have varied the experimental parameters such as temperature and duration of synthesis. Fig. 6(a), 1(c, d) and 6(b) show the FESEM images of the product obtained at 100 °C, 150 °C and 200 °C, respectively, keeping other parameters constant (indium sulfate as the precursor, 30 h duration). At lower synthesis temperature (100 °C), near-spherical microspheres composed of nanoflakes were obtained.

The diameter of these microspheres was measured to be 1–1.5 μm , which is lower than that obtained at 150 °C (3–8 μm). This suggests a slower growth rate at lower synthesis temperature. In addition, these microspheres were found to be not hollow as confirmed from the TEM images (not shown). The formation of hollow microspheres [Fig. 1(c, d)] at 150 °C is discussed in section 3.1. At a higher temperature (200 °C), no spherical structure was found, although the agglomerated features appeared to be composed of nanoflakes, as shown in Fig. 6(b). This suggests that an optimum temperature around 150 °C is needed to obtain hollow microspheres. Fig. 7 shows the FESEM images of the product obtained using indium sulfate at 150 °C by varying reaction duration. At a shorter duration of 8 h [Fig. 7(a, b)], most of the microspheres were found to be not hollow. With increasing the synthesis duration to 15 h, hollowness begins to appear [Fig. 7(c)] and most of the microspheres were found to be hollow at 30 h [Fig. 1(c, d)] and 48 h [Fig. 7(d)]. This process is believed to follow the well-known Ostwald ripening process, causing the formation of hollow spherical structures with an increase in reaction duration.^{31,32} In all of the above experiments, oxalic acid was used as a shape-controlling reagent. To find the exact role of oxalic acid, we carried out an experiment without oxalic acid while keeping the rest of the reaction parameters fixed (indium chloride and L-cystine as indium and sulfur sources, respectively; 150 °C for 30 h). Fig. 8(a) and (b) show FESEM images of agglomerated nanoflakes (without spherical structures) obtained in the absence of oxalic acid at a different magnification. This clearly indicates the role of oxalic acid in the formation of spherical structures. The effective BET surface area and the pore volume [Fig. S3 (ESI[†])] of agglomerated nanoflakes were measured to be 103.05 $\text{m}^2 \text{g}^{-1}$ and 0.387 $\text{cm}^3 \text{g}^{-1}$, respectively, which are lower than those of hollow In_2S_3 microspheres composed of nanoflakes. The pore diameter was measured to be 8.8 Å. However, at a higher synthesis temperature the effect of oxalic acid is found to be negligible [Fig. 6(b)] and/or the breakdown of spherical structures occurs. On the basis of the above results, the growth mechanism can be schematically presented as shown in Fig. 9. The fine particles initially nucleated in the solution can be flocculated to nanoflakes. L-Cystine used as a sulfur source in the present work can act as a complexing agent because of its functional groups $-\text{NH}_2$, $-\text{COOH}$, and $-\text{SH}$ that can react with metal ions.³³ The coordination interaction between In^{3+} and L-cystine can therefore produce the complex.³⁴ Upon formation of thin flake-like

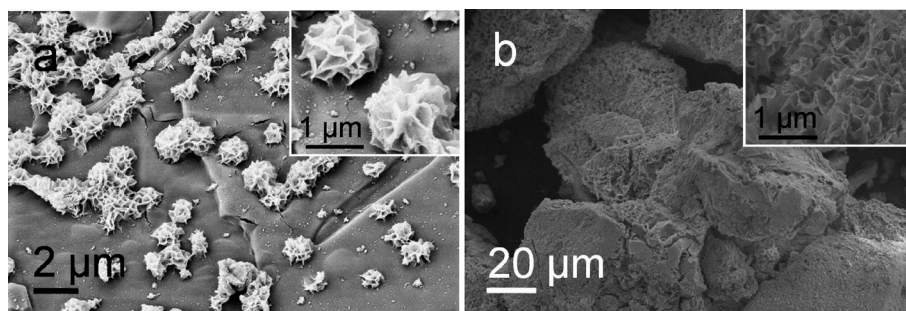


Fig. 6 FESEM images of In_2S_3 obtained at (a) 100 °C and (b) 200 °C using indium sulfate as the indium source while other parameters remained the same.

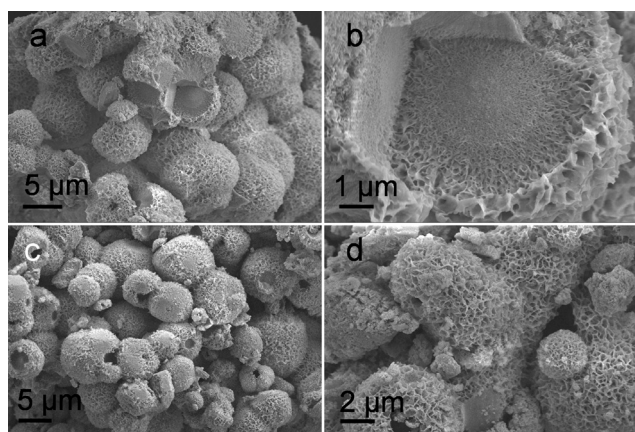


Fig. 7 FESEM images of In_2S_3 microspheres obtained at 150 °C after (a, b) 8 h, (c) 15 h and (d) 48 h using indium sulfate as the indium source while other parameters remained the same.

structures at 150 °C, oxalic acid is suggested to play a role in their assembly to spherical structures, which are Ostwald ripened to hollow structures with an increase in reaction duration. Both indium chloride and indium sulfate precursors produced nanoflakes as the initial building blocks of In_2S_3 microspheres, whereas nanobricks were obtained with indium nitrate as an indium precursor. This indicates that the indium precursor solution plays a role in the nucleation and the subsequent growth of different shapes of the building blocks. Although the indium precursor plays a strong role in the formation of building blocks, *i.e.* nanoflakes and nanobricks, of microspheres, further work is necessary to understand the exact cause behind it.

In order to compare the results obtained by the hydrothermal method with a simple solution process, different indium precursors (0.01 M) were stirred in the aqueous solvent at room temperature, along with L-cystine and oxalic acid. All of the samples show similar fibrous morphology [Fig. S4(a–c), ESI†], although their diameter varies with the indium precursor. The diameters of the fiber were measured to be 150–200 nm, 80–100 nm, and 150–200 nm for the sample prepared with indium chloride, indium sulfate and indium nitrate, respectively. Interestingly, no fibrous morphology [Fig. S4(d), ESI†] was obtained in the absence of oxalic acid with indium sulfate as an indium precursor. This indicates that oxalic acid forms a chain-like complex forming fibrous morphology at room temperature and acts as a shape-controlling agent, which can form a different shape with a change in synthesis process and reaction temperature as observed here. The XRD pattern (Fig. S5, SI†) of the fibrous product obtained with indium sulfate indicates the crystalline nature of the product. However, the XRD pattern neither matches any expected products such as InS , In_2S_3 , $\text{In}_2(\text{SO}_4)_3$ nor any known product. Further investigation is needed to identify the crystal structure of the product.

3.6. Photocatalytic study

The photocatalytic performance of as-synthesized In_2S_3 microspheres was tested for the degradation of MB and CV using UV-vis absorption spectroscopy. Fig. 10(a) shows a typical UV-vis absorption spectra of MB solution in the presence of In_2S_3 hollow microspheres (obtained with indium sulfate)

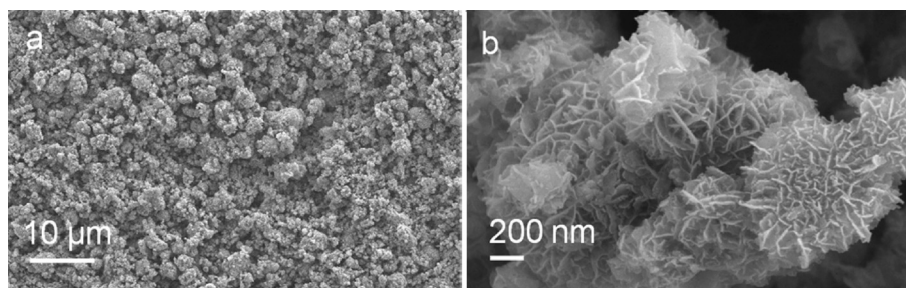


Fig. 8 FESEM images at (a) Low and (b) high magnification, of In_2S_3 nanoflakes in the absence of oxalic acid while keeping the rest of parameters constant.

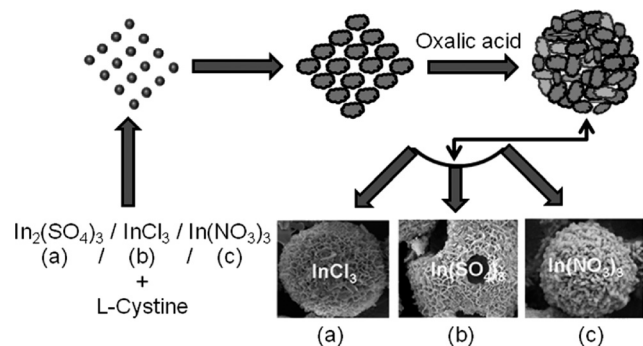


Fig. 9 Schematic of the formation of In_2S_3 microspheres from different precursors using the hydrothermal synthesis process.

irradiated by visible light for different durations. Prior to irradiation, the catalyst dispersed dye solution was kept in the dark for 30 min for the complete adsorption–desorption of dyes on the catalyst surface. Fig. 10(b) shows the degradation of MB in the absence and presence of In_2S_3 microspheres obtained from different precursors as a function of visible light irradiation time. For comparison, degradation was also performed with standard P-25 TiO_2 nanoparticles. In the absence of In_2S_3 , there was no change in the concentration of the dye for 6 h irradiation, indicating that light alone is not adequate for the degradation of the dye. With In_2S_3 , the concentration of MB was found to decrease as a function of irradiation time. MB degradation efficiency $[(C_0 - C)/C_0 \times 100]$ was found to be higher with microspheres obtained from indium sulfate (97.21%) than those obtained from indium chloride (83.07%) and indium nitrate (71.28%) in 6 h

irradiation. Here C_0 and C are the dye concentrations before and after irradiation, respectively. In the same irradiation time of 6 h, the degradation efficiency of standard P-25 TiO_2 nanoparticles was measured to be 81.94%, which is lower than that obtained with hollow In_2S_3 microspheres composed of nanoflakes. This could be due to the higher band gap of TiO_2 nanoparticles leading to less absorption of visible light. The present MB degradation efficiency obtained with In_2S_3 microspheres using an incandescent lamp is much higher than the degradation efficiency (61.2%) obtained with In_2S_3 nanobelts UV irradiated for 8 h.¹⁰ The MB degradation rate constant was calculated from the linear plot of $\ln(C_0/C)$ vs. irradiation time as shown in Fig. 10(c). The rate constant was found to be in the order of 0.0085 min^{-1} (hollow In_2S_3 microspheres composed of nanoflakes), $>0.0046 \text{ min}^{-1}$ (solid In_2S_3 microspheres composed of nanoflakes), $>0.0041 \text{ min}^{-1}$ (P-25 TiO_2) and $>0.0032 \text{ min}^{-1}$ (solid In_2S_3 microspheres composed of brick-like structures). Fig. 10(d) shows the CV degradation efficiency of In_2S_3 microspheres obtained with different indium precursors, without In_2S_3 microspheres and with P-25 TiO_2 for comparison. The corresponding linear plots of $\ln(C_0/C)$ vs. irradiation time of CV degradation are shown in Fig. 10(e). The rate constant (and efficiency) for the degradation of CV was measured to be 0.079 min^{-1} (90.33%), 0.097 min^{-1} (95.43%), and 0.067 min^{-1} (85.32%) for the In_2S_3 microspheres obtained from indium chloride, indium sulfate and indium nitrate precursors, respectively, and 0.009 min^{-1} (26.93%) for P-25 TiO_2 . It clearly shows that both MB and CV degradation performance of In_2S_3 microspheres obtained from indium sulfate precursor are the highest, which is due

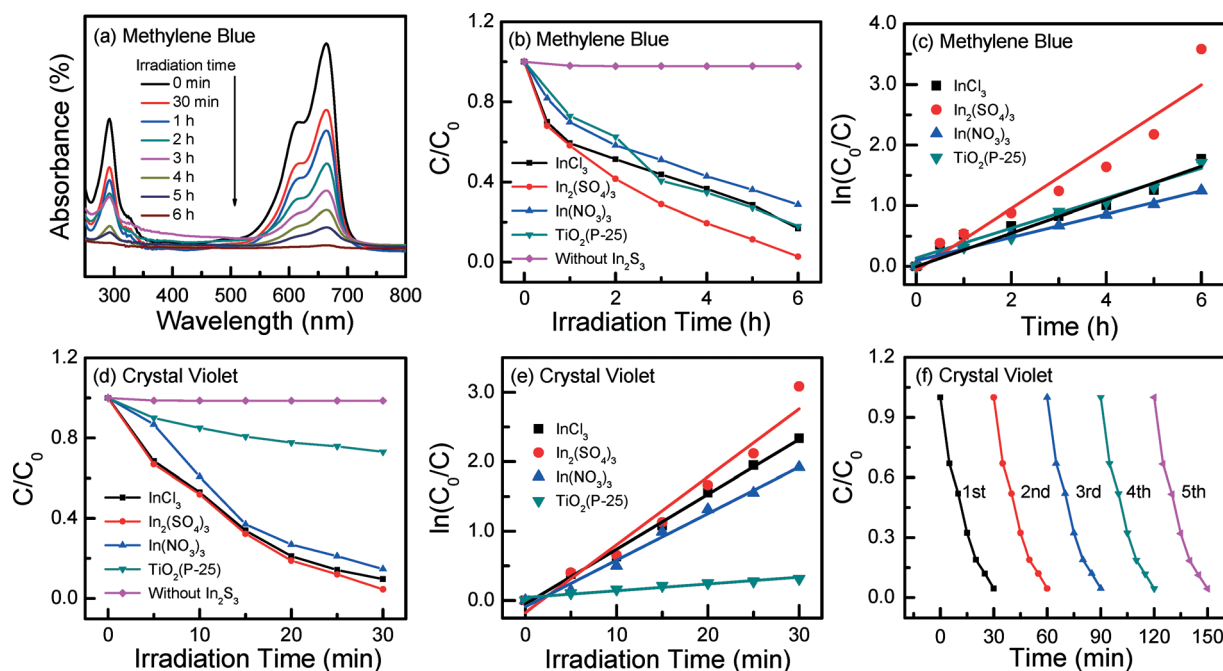


Fig. 10 (a) UV-vis absorption spectra of MB solution irradiated for different durations with hollow In_2S_3 microspheres obtained using indium sulfate precursor. (b, d) The photodegradation performance and (c, e) the linearly fitted curve for MB and CV as a function of irradiation time with In_2S_3 microspheres synthesized using different indium precursors. (f) The performance of hollow In_2S_3 microspheres for the photodegradation of CV for 5 cycles.

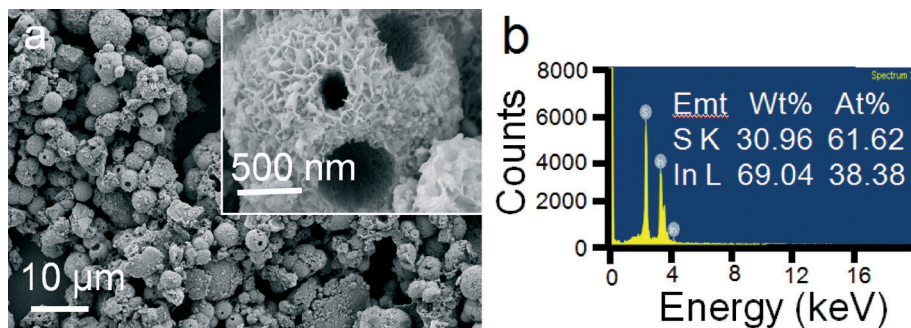


Fig. 11 (a) FESEM images and (b) an EDX pattern of hollow In_2S_3 microspheres after five cycles of CV degradation.

to their hollow nature and hence larger interfacial surface area. The lowest performance was obtained from solid In_2S_3 microspheres composed of nanobricks because of their low BET surface area. In addition, we have tested the photocatalytic properties of agglomerated nanoflakes obtained using indium sulfate without oxalic acid, and the CV degradation efficiency of 83.03% was found to be lower than that of hollow microspheres (95.43%) obtained with oxalic acid. This is due to the lower effective BET surface area of agglomerated nanoflakes.

We further studied the durability and the efficiency of hollow In_2S_3 microspheres obtained with indium sulfate upon degradation of CV for five cycles. Fig. 10(f) shows degradation efficiency as a function of cycles, with each cycle running for 30 min. Degradation performance was measured to be 95.69%, 95.65%, 95.61%, 95.53% and 95.5% after the first, second, third, fourth and fifth cycles, respectively, indicating a negligible change in degradation performance and high stability of the catalyst. After the five cycles of the degradation experiment, we collected the catalyst powder by centrifugation and dried it at 60 °C for 4 h. Fig. 11(a) confirms that the morphology of hollow microspheres remains the same after being used in the photocatalytic experiments for 2.5 h. The stoichiometric ratio of S to In remains approximately the same, *i.e.* 1.6 as shown in Fig. 11(b). The phase of used catalyst powder remains unchanged (XRD pattern not shown).

The photocatalytic degradation of organic chemicals usually follows the formation of hydroxyl radicals upon light irradiation. In order to confirm the formation of hydroxyl radicals, we have used a simple terephthalic acid (TA) test using photoluminescence spectroscopy. TA reacts immediately with hydroxyl radical forming 2-hydroxyterephthalic acid (HTA), which shows an intense luminescence peak at 426 nm. Fig. 12 shows the photoluminescence spectra of TA solution mixed with In_2S_3 hollow microspheres at different light irradiation durations. Initially (without light irradiation), no luminescence feature was observed, indicating the absence of HTA in the solution. With an increase in the duration of light irradiation, luminescence intensity was found to increase linearly (inset Fig. 12). This suggests the linear increase of HTA concentration, which is proportional to the formation of the hydroxyl radical.

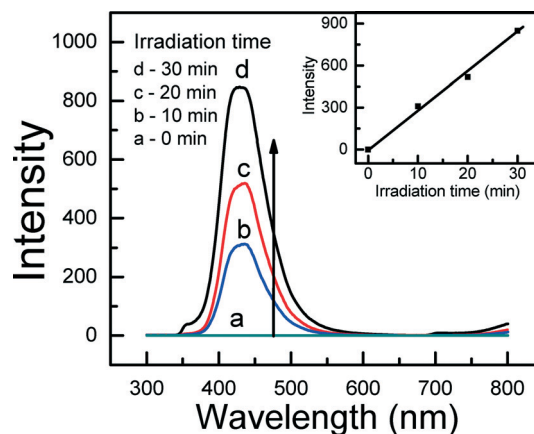


Fig. 12 Photoluminescence spectra of terephthalic acid solution mixed with In_2S_3 hollow microspheres by varying light irradiation duration.

4. Conclusions

In summary, we successfully synthesized tetragonal In_2S_3 microspheres composed of nanoflakes and nanobricks using a template-free and surfactant-less hydrothermal method. The indium precursors were found to play an important role in controlling the morphology of the In_2S_3 product. The use of the biomolecule L-cystine as a sulfur source makes the present synthesis process greener and attractive. The highest photocatalytic performance was obtained from hollow microspheres due to their larger effective surface area. The recycling ability of the catalyst powder was tested and found to be stable without a change in morphology and phase after five cycles. A simple TA test using photoluminescence spectroscopy confirmed that the hydroxyl radical acts as an active species for the degradation of organic chemicals.

Acknowledgements

This work was supported by the Department of Science and Technology, New Delhi, India through the INT/Korea/P-02 grant and the National Research Foundation of Korea, MEST (NRF-2011-0025386).

References

- 1 M. Pelaez, N. T. Nolan, S. C. Pillai, M. K. Seery, P. Falaras, A. G. Kontos, P. S. M. Dunlop, J. W. J. Hamilton, J. A. Byrne, K. O'Shea, M. H. Entezari and D. D. Dionysiou, *Appl. Catal., B*, 2012, **125**, 331–349.
- 2 Z. Li, Y. Shen, Y. Guan, Y. Hu, Y. Lin and C.-W. Nan, *J. Mater. Chem. A*, 2014, **2**, 1967–1973.
- 3 M. M. Khan, S. A. Ansari, D. Pradhan, M. O. Ansari, D. H. Han, J. Lee and M. H. Cho, *J. Mater. Chem. A*, 2014, **2**, 637–644.
- 4 W.-T. Kim and C.-D. Kim, *J. Appl. Phys.*, 1986, **60**, 2631–2633.
- 5 A. Timoumi, H. Bouzouita, M. Kanzari and B. Rezig, *Thin Solid Films*, 2005, **124–128**, 480–481.
- 6 Y.-J. Hsiao, C.-H. Lu, L.-W. Ji, T.-H. Meen, Y.-L. Chen and H.-P. Chi, *Nanoscale Res. Lett.*, 2014, **9**, 32.
- 7 R. Diehl and R. Nitsche, *J. Cryst. Growth*, 1975, **28**, 306–310.
- 8 N. Naghavi, S. Spiering, M. Powalla, B. Cavana and D. Lincot, *Prog. Photovoltaics*, 2003, **11**, 437–443.
- 9 Y. He, D. Li, G. Xiao, W. Chen, Y. Chen, M. Sun, H. Huang and X. Fu, *J. Phys. Chem. C*, 2009, **113**, 5254–5262.
- 10 W. Du, J. Zhu, S. Li and X. Qian, *Cryst. Growth Des.*, 2008, **8**, 2130–2136.
- 11 S. Cingarapu, M. A. Ikenberry, D. B. Hamal, C. M. Sorensen, K. Hohn and K. J. Klabunde, *Langmuir*, 2012, **28**, 3569–3575.
- 12 L. Y. Chen, Z. D. Zhang and W. Z. Wang, *J. Phys. Chem. C*, 2008, **112**, 4117–4123.
- 13 Y. Liu, M. Zhang, Y. Gao, R. Zhang and Y. Qian, *Mater. Chem. Phys.*, 2007, **101**, 362–366.
- 14 W. Zhang, D. K. Ma, Z. Huang, Q. Tang, Q. Xie and Y. T. Qian, *J. Nanosci. Nanotechnol.*, 2005, **5**, 776–780.
- 15 X. Chen, Z. Zhang, X. Zhang, J. Liu and Y. Qian, *Chem. Phys. Lett.*, 2005, **407**, 482–486.
- 16 X. Fu, X. Wang, Z. Chen, Z. Zhang, Z. Li, D. Y. C. Leung, L. Wu and X. Fu, *Appl. Catal., B*, 2010, **95**, 393–399.
- 17 C. R. Patra, S. Patra, A. Gabashvili, Y. Mastai, Y. Gedanken, A. Palchik and M. A. Slifkin, *J. Nanosci. Nanotechnol.*, 2006, **6**, 845–851.
- 18 S. Gorai and S. Chaudhuri, *Mater. Chem. Phys.*, 2005, **89**, 332–335.
- 19 P. Gao, Y. Xie, S. Chen and M. Zhou, *Nanotechnology*, 2006, **17**, 320.
- 20 Y. Nosaka, N. Ohta and H. Miyama, *J. Phys. Chem.*, 1990, **94**, 3752–3755.
- 21 K. H. Park, K. Jang and S. U. Son, *Angew. Chem., Int. Ed.*, 2006, **45**, 4608–4612.
- 22 Y. Xiong, Y. Xie, G. Du and X. Tian, *J. Mater. Chem.*, 2002, **1**, 98–102.
- 23 W. Chen, J. O. Bovin, A. G. Joly, S. Wang, F. Su and G. Li, *J. Phys. Chem. B*, 2004, **108**, 11927–11934.
- 24 X. Zhu, J. Ma, Y. Wang, J. Tao, J. Zhou, Z. Zhao, L. Xie and H. Tian, *Mater. Res. Bull.*, 2006, **41**, 1584–1588.
- 25 D. P. Dutta, G. Sharma, A. K. Tyagi and S. K. Kulshreshtha, *Mater. Sci. Eng., B*, 2007, **138**, 60–64.
- 26 P. Zhao, T. Huang and K. Huang, *J. Phys. Chem. C*, 2007, **111**, 12890–12897.
- 27 X. Ana, J. C. Yu, F. Wang, C. Li and Y. Li, *Appl. Catal., B*, 2013, **129**, 80–88.
- 28 Y. Liu, H. Xu and Y. Qian, *Cryst. Growth Des.*, 2006, **6**, 1304–1307.
- 29 L. Liu, H. Liu, H.-Z. Kou, Y. Wang, Z. Zhou, M. Ren, M. Ge and X. He, *Cryst. Growth Des.*, 2009, **9**, 113–117.
- 30 D. P. Dutta, G. Sharma, S. Ghoshal, N. Kushwah and V. K. Jain, *J. Nanosci. Nanotechnol.*, 2006, **6**, 235–240.
- 31 M. Cao, H. Lian and C. Hu, *Nanoscale*, 2010, **2**, 2619–2623.
- 32 J. Li and H. C. Zeng, *J. Am. Chem. Soc.*, 2007, **129**, 15839–15847.
- 33 P. Zhao, T. Huang and K. Huang, *J. Phys. Chem. C*, 2007, **111**, 12890–12897.
- 34 L.-Y. Chen, Z.-D. Zhang and W.-Z. Wang, *J. Phys. Chem. C*, 2008, **112**, 4117–4123.